

# Flows of gas through a protoplanetary gap

Simon Casassus<sup>1</sup>, Gerrit van der Plas<sup>1</sup>, Sebastian Perez M<sup>1</sup>, William R. F. Dent<sup>2,3</sup>, Ed Fomalont<sup>4</sup>, Janis Hagelberg<sup>5</sup>, Antonio Hales<sup>2,4</sup>, Andrés Jordán<sup>6</sup>, Dimitri Mawet<sup>3</sup>, Francois Ménard<sup>7,8</sup>, Al Wootten<sup>4</sup>, David Wilner<sup>9</sup>, A. Meredith Hughes<sup>10</sup>, Matthias R. Schreiber<sup>11</sup>, Julien H. Girard<sup>3</sup>, Barbara Ercolano<sup>12</sup>, Hector Canovas<sup>11</sup>, Pablo E. Román<sup>13</sup> & Vachail Salinas<sup>1</sup>

**The formation of gaseous giant planets is thought to occur in the first few million years after stellar birth. Models<sup>1</sup> predict that the process produces a deep gap in the dust component (shallower in the gas<sup>2–4</sup>). Infrared observations of the disk around the young star HD 142527 (at a distance of about 140 parsecs from Earth) found an inner disk about 10 astronomical units (AU) in radius<sup>5</sup> (1 AU is the Earth–Sun distance), surrounded by a particularly large gap<sup>6</sup> and a disrupted<sup>7</sup> outer disk beyond 140 AU. This disruption is indicative of a perturbing planetary-mass body at about 90 AU. Radio observations<sup>8,9</sup> indicate that the bulk mass is molecular and lies in the outer disk, whose continuum emission has a horseshoe morphology<sup>8</sup>. The high stellar accretion rate<sup>10</sup> would deplete the inner disk<sup>11</sup> in less than one year, and to sustain the observed accretion matter must therefore flow from the outer disk and cross the gap. In dynamical models, the putative protoplanets channel outer-disk material into gap-crossing bridges that feed stellar accretion through the inner disk<sup>12</sup>. Here we report observations of diffuse CO gas inside the gap, with denser HCO<sup>+</sup> gas along gap-crossing filaments. The estimated flow rate of the gas is in the range of  $7 \times 10^{-9}$  to  $2 \times 10^{-7}$  solar masses per year, which is sufficient to maintain accretion onto the star at the present rate.**

The HD 142527 system offers an unhindered view of its large central gap, and is a promising ‘laboratory’ in which to observe the ongoing formation of gaseous giant planets. The orientation of the disk is well understood. Multiwavelength data are consistent with an inclination of about 20°, indicating that the disk is almost face-on to our line of sight<sup>11</sup>. The disk position angle is about –20° east of north, and the eastern side is the far side of the disk, as suggested by a clear view of the outer disk’s inner rim in the mid-infrared spectral range<sup>11,13</sup> and by a clockwise rotation suggested by what is probably a trailing spiral arm to the west<sup>6</sup>.

We find that the CO(3–2) emission (that is, emission of CO with  $J = 3-2$ , where  $J$  is the CO rotational quantum number) peaks inside the gap. Other disks have been observed to have a CO decrement within dust cavities<sup>14,15</sup>, and may represent later evolutionary stages or different gap-clearing mechanisms. Gas inside dust cavities has previously been directly observed very close to the central star (inside the dust evaporation radius) using near-infrared interferometry<sup>16–18</sup>. Other indirect observations of gas inside<sup>19–23</sup> dust gaps at larger distances from the central star have revealed spectroscopically resolved gas tracers, such as rovibrational CO emission at a wavelength of 4.67 μm and [O I] emission at 6,300 Å, under the assumption of azimuthal symmetry and Keplerian rotation. Spectro-astrometry in combination with Keplerian disk models and azimuthal symmetry have also been used to infer the presence of CO gas inside disk gaps<sup>24–26</sup>. Our data provide a well-resolved observation of gas at sub-millimetre wavelengths inside a dust gap.

The dust gap that we see in the radio continuum (Fig. 1a) indicates a decrease by a factor of at least 300 in the surface density of millimetre-sized grains, judging from the contrast ratio between the peak on the horseshoe-shaped outer disk (the northern flux peak at 360 mJy per beam) and the faintest detected signal inside the gap (namely the western filament at 1 mJy per beam; see below). Yet there is no counterpart in the CO(3–2) map (Fig. 1b) of the arc that we see in the radio continuum. CO(3–2) is probably optically thick, as reflected by its diffuse morphology, so that it traces the temperature profile rather than the underlying density field. Detailed modelling of optically thin isotopologue data is required to constrain accurately the depth of the gaseous gap. To study the distribution of dense gas inside the gap, we use the tracer HCO<sup>+</sup>.

The second result from our observations is that gas showing HCO<sup>+</sup>(4–3) emission, expected in the denser regions (molecular hydrogen number density,  $n_{\text{H}_2} \approx 10^6 \text{ cm}^{-3}$ ) exposed to ultraviolet radiation, is indeed found in the exposed rim of the dense outer disk, but also along gap-crossing filaments. The most conspicuous filament extends eastwards from the star, and a fainter filament extends westwards. Both filaments subtend an angle of about  $140 \pm 10^\circ$  with the star at its vertex. The central regions of these filaments correspond to the brightest features in the HCO<sup>+</sup> line intensity maps (Fig. 1c), although the outer disk is brighter in peak specific intensity (Supplementary Fig. 7). Thus, line velocity profiles are broader on the stellar side of the filaments than in the outer disk, where they merge with the outer-disk Keplerian rotation pattern. These narrow, systemic-velocity HCO<sup>+</sup> filaments are best seen in intensity maps integrated over the filament velocities (Fig. 1d, inset). No central peak is seen in the channel maps (Supplementary Fig. 2), and so a beam-elongation effect can be ruled out. The eastern filament also is notable in terms of peak HCO<sup>+</sup> specific intensity (Supplementary Fig. 7e). For ease of visualization, we show deconvolved models of the HCO<sup>+</sup> intensity images in the inset to Fig. 1d. A related feature is seen in CO(3–2) emission, whose intensity peaks in the more diffuse regions surrounding the eastern HCO<sup>+</sup> filament. We note from the inset to Fig. 1 that the continuum also shows features under the HCO<sup>+</sup> filament. These features are faint and grow away from the edges of the horseshoe-shaped outer disk. Estimates of physical conditions are given in Supplementary Information.

The molecular and filamentary flows near the star are non-Keplerian. Blueshifted emission extends to the east from the central intensity peak (Fig. 1d). This velocity component is broad near the star, with emission ranging from –3.4 to +11 km s<sup>–1</sup> (Supplementary Fig. 2), and is marginally resolved (the central HCO<sup>+</sup> peak extends over about  $0.65 \times 0.38 \text{ arcsec}^2$ ). In the deconvolved images of the inset to Fig. 1d, the peak intensity in the blue- and red-outlined regions are separated by about 0.2 arcsec, that is, by the diameter of the inner disk,

<sup>1</sup>Departamento de Astronomía, Universidad de Chile, Casilla 36-D, Santiago, Chile. <sup>2</sup>Joint ALMA Observatory, Alonso de Córdova 3107, Vitacura 763-0355, Santiago, Chile. <sup>3</sup>European Southern Observatory, Casilla 19001, Vitacura, Santiago, Chile. <sup>4</sup>National Radio Astronomy Observatory, 520 Edgemont Road, Charlottesville, Virginia 22903-2475, USA. <sup>5</sup>Observatoire de Genève, Université de Genève, 51 Chemin des Maillettes, 1290, Versoix, Switzerland. <sup>6</sup>Departamento de Astronomía y Astrofísica, Pontificia Universidad Católica de Chile, Santiago, Chile. <sup>7</sup>UMI-FCA, CNRS/INSU France (UMI 3386), and Departamento de Astronomía, Universidad de Chile, Santiago, Chile. <sup>8</sup>CNRS/UJF Grenoble 1, UMR 5274, Institut de Planétologie et d’Astrophysique de Grenoble (IPAG), F-48041 Grenoble Cedex 9, France. <sup>9</sup>Harvard-Smithsonian Center for Astrophysics, 60 Garden Street, Cambridge, Massachusetts 02138, USA. <sup>10</sup>Department of Astronomy, UC Berkeley, 601 Campbell Hall, Berkeley, California 94720, USA. <sup>11</sup>Departamento de Física y Astronomía, Universidad Valparaíso, Avenida Gran Bretaña 1111, Valparaíso, Chile. <sup>12</sup>University Observatory, Ludwig-Maximilians University, D-81679 Munich, Germany. <sup>13</sup>Center of Mathematical Modeling, University of Chile, Avenida Blanco Encalada 2120 Piso 7, Santiago, Chile.

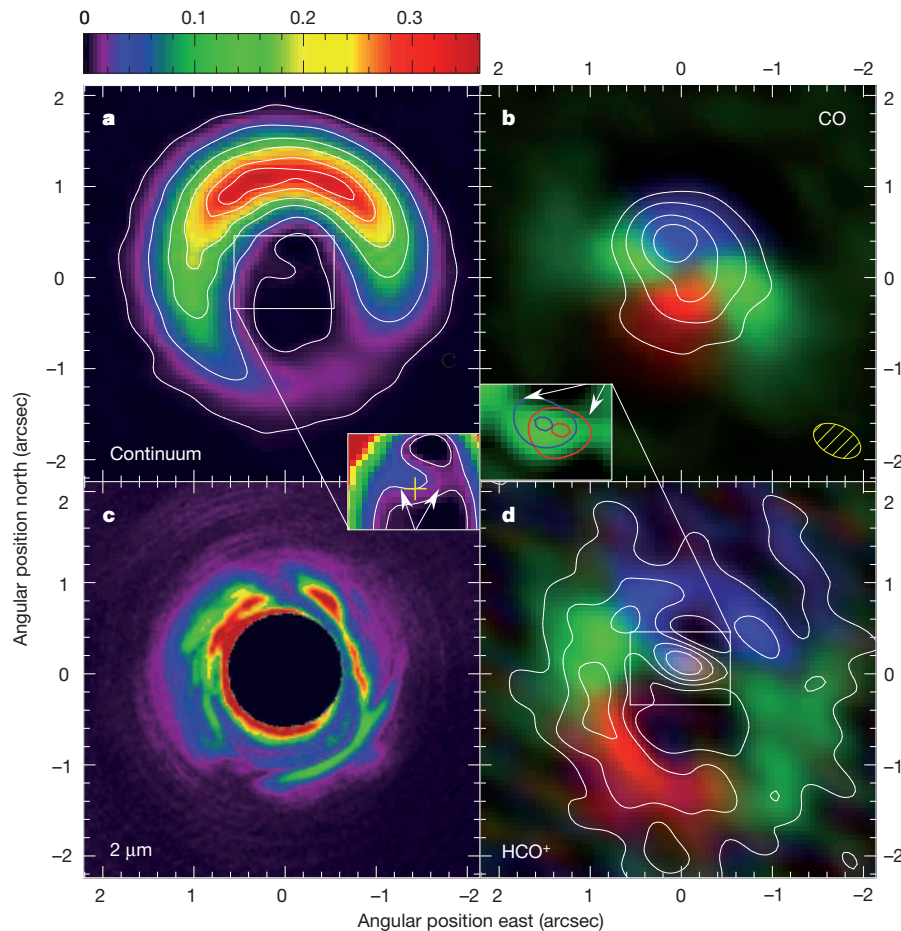


**Figure 1 | ALMA observations of HD 142527, with a horseshoe dust continuum surrounding a gap that still contains gas.** We see diffuse CO gas in Keplerian rotation (coded in Doppler-shifted colours), and filamentary emission in  $\text{HCO}^+$ , with non-Keplerian flows near the star (comparison models illustrative of Keplerian rotation are shown in Supplementary Information). The near-infrared emission abuts the inner rim of the horseshoe-shaped outer disk. The star is at the origin of the coordinates. North is up and east is to the left. **a**, Continuum at 345 GHz, with specific intensity units in Janskys per beam. It is shown on an exponential scale (colour scale). A beam ellipse is shown in the bottom right of **b**, and contours are drawn at 0.01, 0.1, 0.3, 0.5, 0.75 and 0.9 times the peak value. The noise level is  $1\sigma = 0.5$  mJy per beam. **b**, CO(3–2) line intensity shown by white contours at fractions of 0.3, 0.5, 0.75 and 0.95 of the peak intensity value,  $2.325 \times 10^{-20}$  W per beam. The underlying red–green–blue image also shows CO(3–2) line intensity, but integrated in three different velocity bands, whose velocity limits are indicated in the spectra of Supplementary Fig. 8. **c**, Near-infrared image from Gemini that traces reflected stellar light, shown on a linear scale. We applied a circular intensity mask to the stellar glare, some of which immediately surrounds the mask. See

and at a position angle orthogonal to that expected from close-in high-velocity material in Keplerian rotation. Very blueshifted emission could reach out to 0.2 arcsec from the star (channel at  $-2.4 \text{ km s}^{-1}$  in Supplementary Fig. 2, taking into account the beam). A blueshifted CO(3–2) high-velocity component can also be seen at the base of this feature, near the star (at  $-2.1 \text{ km s}^{-1}$  in Supplementary Fig. 5).

The non-Keplerian  $\text{HCO}^+$  is probably not consistent with a central outflow. Stellar outflows are not observed<sup>27</sup> in disks with inner cavities and no molecular envelopes (that is, transition disks). For an outflow orientation, the low velocities measured by the lines imply that the filaments in HD 142527 would stand still and hover above the star (Supplementary Information, section 3). Even the blueshifted emission is slow by comparison with the escape velocity. A slow disk wind (for example one photoevaporative or magnetically driven) can also be excluded on the basis of the high collimation shown by the  $\text{HCO}^+$

Supplementary Fig. 1 for an overlay with the continuum. **d**,  $\text{HCO}^+$  (4–3) line intensity shown by white contours at fractions of 0.1, 0.3, 0.5, 0.75 and 0.95 of the peak intensity value,  $0.40 \times 10^{-20}$  W per beam, overlaid on a red–green–blue image of  $\text{HCO}^+$  intensity summed in three different colour bands (see Supplementary Fig. 8 for definitions). Insets show magnified views of the central features that cross the dust gap. The cross indicates the star at the origin, with a precision of 0.05 arcsec, and the arrows point at the filaments. Inset to **a**: same as in **a**, with a narrow exponential scale highlighting the gap-crossing filaments. These features appear to grow from the eastern and western sides of the horseshoe. Contours are at 0.0015 and 0.005 Janskys per beam. Inset to **d**: deconvolved models (Supplementary Information) of the  $\text{HCO}^+$  emission (green) at velocities where the gap-crossing filaments are seen, that is, from  $3.2$  to  $4.3 \text{ km s}^{-1}$ . Intensity maps for the blue and red velocity ranges (see Supplementary Fig. 8 for definitions) are shown in contours, with levels at 0.5 and 0.95 times the peak values. These red and blue contours are an alternative way to present the intensity field shown in **d**, but deconvolved for ease of visualization.

emission. Indeed, the CO 4.67- $\mu\text{m}$  emission seen in the inner disk<sup>26</sup> is purely Keplerian, it does not bear the signature of the disk winds seen in other systems and its orientation is the same as that of the outer disk. An orthogonal inner disk can also be discounted on dynamical grounds (Supplementary Information, section 3).

It is natural to interpret the filaments as planet-induced gap-crossing accretion flows, or ‘bridges’. Because the eastern side is the far side, the blueshifted part of the eastern bridge is directed towards the star and is a high-velocity termination of the accretion flow onto the inner disk. These bridges are predicted by hydrodynamical simulations when applied to planet-formation feedback in HD 142527 (ref. 7). In these simulations, the bridges straddle the protoplanets responsible for the dynamical clearing of the large gap in HD 142527. They are close to Keplerian rotation in azimuth, but have radial velocity components of  $\geq 0.1$  of the azimuthal components. In our data, we see that

as the bridges contact the inner disk they also coincide with higher-velocity material, at two-dimensional radial velocities less than their azimuthal velocities in the plane of the sky.

An interesting comparison object is the GG Tau circumbinary disk. A submillimetre continuum accretion stream<sup>28</sup> is seen to cross the gap that surrounds the central binary in GG Tau, with indications of shocked infrared molecular gas in the inner disk<sup>29</sup>. The angular radii of the rings in GG Tau and in HD 142527 are very similar, as are the morphologies of the GG Tau streamer and the eastern filament (although it is fainter relative to the outer disk in HD 142527). However, the GG Tau binary has a mass ratio of about 1, a separation of 0.25 arcsec and is aligned along the streamer, whereas in HD 142527 no stellar companion has been detected (see Supplementary Information for limits; mass ratios are  $>10$  at 0.088 arcsec). The putative companions responsible for the streams in HD 142527 are of much lower mass than in GG Tau.

We performed high-contrast infrared imaging to attempt the detection of the possible accreting protoplanets that would be expected if the gap-crossing bridges observed in  $\text{HCO}^+$  are indeed planet-induced gap-crossing accretion flows. Neglecting extinction, we could virtually rule out any companion more than about four times as massive as Jupiter, at a separation of 0.3–2.5 arcsec (Supplementary Information, section 4, and Supplementary Fig. 13, which also concerns the lack of close stellar companions). However, according to the hydrodynamical simulations the channelling protoplanets should be located inside the gap-crossing bridges. Our estimates for the hydrogen column number density,  $N_{\text{H}}$ , along the bridges correspond to a broad range of high visual ( $\sim 5,500 \text{ \AA}$ ) extinction values,  $5 \text{ mag} \lesssim A_V \lesssim 50 \text{ mag}$ , for standard dust abundances. Any protoplanets embedded inside the bridges, and certainly those embedded in the dense horseshoe structure, will be obscured, and our mass limits will be correspondingly increased.

As well as the diffuse gas inside the gap and the gap-crossing filaments, a third feature of our observations is the horseshoe shape of the continuum, which was seen previously by the Submillimeter Array<sup>8</sup>, Hawaii, but at coarser resolutions, and whose origin is still unclear. The millimetre continuum traces the total dust mass, so the north–south specific intensity ratio of  $28 \pm 0.5$  reflects the underlying dust mass asymmetry. At its peak, the continuum may even be optically thick, as it coincides with a decrease in the  $\text{HCO}^+$  emission. For a constant gas-to-dust mass ratio, such horseshoe-shaped mass asymmetries arise in models of planet-induced dynamical clearing. In general, these horseshoes can be produced by Rossby-wave instabilities, which are seen in high-resolution, three-dimensional simulations at the edge of sharp density gradients (P. Varnière, personal communication). However, horseshoes have also been modelled in the context of large-scale vortices induced by sharp viscosity gradients<sup>30</sup>.

Another interpretation of the horseshoe continuum is that it results from a varying dust-to-gas ratio and azimuthal grain-size segregation. By contrast to the continuum, the outer disk is seen as a whole ring in  $\text{HCO}^+$  (Supplementary Fig. 7), which is a tracer of dense gas, and is probably optically thick along the ring. A rarefaction of millimetre-sized dust grains to the south could perhaps explain the lack of a submillimetre continuum. Only small dust grains would be found in the south. These small grains efficiently scatter the near-infrared light seen in Fig. 1c, filling the opening of the horseshoe. However, azimuthal dust segregation has been predicted for centimetre-sized grains at co-rotation in two-fluid simulations of gap clearing by giant-planet formation<sup>2</sup>, whereas millimetre-sized grains remain relatively unaffected. We explain in Supplementary Information why differential stellar heating cannot account for the observed north–south contrast.

The filamentary flows and the residual gas inside the gap are in qualitative agreement with planet-formation feedback on the parent disk, which feedback carves a gap in the dust distribution while still feeding stellar accretion through gap-crossing accretion streams. As

detailed in Supplementary Information, the observed inflow velocity, together with the critical density of the molecular tracer and the section of the filaments, provide a lower bound to the mass inflow rate of  $7 \times 10^{-9} M_{\odot} \text{ yr}^{-1}$ . An upper bound of  $2 \times 10^{-7} M_{\odot} \text{ yr}^{-1}$  can be estimated from the continuum mass in the filaments and their kinematic timescale. These estimates for the mass inflow rate are close to the observed stellar accretion rate<sup>10</sup>, of  $7 \times 10^{-8} M_{\odot} \text{ yr}^{-1}$ , giving quantitative support to our suggestion that the  $\text{HCO}^+$  filaments are inflows.

Received 12 August; accepted 31 October 2012.

Published online 2 January; corrected online 9 January 2013 (see full-text HTML version for details).

- Lubow, S. H. & D'Angelo, G. Gas flow across gaps in protoplanetary disks. *Astrophys. J.* **641**, 526–533 (2006).
- Fouchet, L., Gonzalez, J.-F. & Maddison, S. T. Planet gaps in the dust layer of 3D protoplanetary disks. I. Hydrodynamical simulations of T Tauri disks. *Astron. Astrophys.* **518**, A16 (2010).
- Ayliffe, B. A., Laibe, G., Price, D. J. & Bate, M. R. On the accumulation of planetesimals near disc gaps created by protoplanets. *Mon. Not. R. Astron. Soc.* **423**, 1450–1462 (2012).
- Zhu, Z., Nelson, R. P., Hartmann, L., Espaillat, C. & Calvet, N. Transitional and pretransitional disks: gap opening by multiple planets? *Astrophys. J.* **729**, 47–58 (2011).
- van Boekel, R. *et al.* The building blocks of planets within the 'terrestrial' region of protoplanetary disks. *Nature* **432**, 479–482 (2004).
- Fukagawa, M. *et al.* Near-infrared images of protoplanetary disk surrounding HD 142527. *Astrophys. J.* **636**, L153–L156 (2006).
- Casassus, S. *et al.* The dynamically disrupted gap in HD 142527. *Astrophys. J.* **754**, L31–L35 (2012).
- Ohashi, N. Observational signature of planet formation: the ALMA view. *Astrophys. Space Sci.* **313**, 101–107 (2008).
- Oberg, K. I. *et al.* Disk imaging survey of chemistry with SMA. II. Southern sky protoplanetary disk data and full sample statistics. *Astrophys. J.* **734**, 98–109 (2011).
- García Lopez, R., Natta, A., Testi, L. & Habart, E. Accretion rates in Herbig Ae stars. *Astron. Astrophys.* **459**, 837–842 (2006).
- Verhoeff, A. P. *et al.* The complex circumstellar environment of HD 142527. *Astron. Astrophys.* **528**, A91–A103 (2011).
- Dodson-Robinson, S. E. & Salyk, C. Transitional disks as signposts of young, multiplanet systems. *Astrophys. J.* **738**, 131–145 (2011).
- Fujiwara, H. *et al.* The asymmetric thermal emission of the protoplanetary disk surrounding HD 142527 seen by Subaru/COMICS. *Astrophys. J.* **644**, L133–L136 (2006).
- Lyo, A.-R., Ohashi, N., Qi, C., Wilner, D. J. & Su, Y.-N. Millimeter observations of the transition disk around HD 135344B (SAO 206462). *Astron. J.* **142**, 151–160 (2011).
- Mathews, G. S., Williams, J. P. & Ménard, F. 880  $\mu\text{m}$  imaging of a transitional disk in Upper Scorpius: holdover from the era of giant planet formation? *Astrophys. J.* **753**, 59–70 (2012).
- Tatulli, E. *et al.* Constraining the wind launching region in Herbig Ae stars: AMBER/VLT spectroscopy of HD 104237. *Astron. Astrophys.* **464**, 55–58 (2007).
- Kraus, S. *et al.* The origin of hydrogen line emission for five Herbig Ae/Be stars spatially resolved by VLT/AMBER spectro-interferometry. *Astron. Astrophys.* **489**, 1157–1173 (2008).
- Eisner, J. A. *et al.* Spatially and spectrally resolved hydrogen gas within 0.1 AU of T Tauri and Herbig Ae/Be Stars. *Astrophys. J.* **718**, 774–794 (2010).
- Carr, J. S., Mathieu, R. D. & Najita, J. R. Evidence for residual material in accretion disk gaps: CO fundamental emission from the T Tauri spectroscopic binary DQ Tauri. *Astrophys. J.* **551**, 454–460 (2001).
- Najita, J., Carr, J. S. & Mathieu, R. D. Gas in the terrestrial planet region of disks: CO fundamental emission from T Tauri Stars. *Astrophys. J.* **589**, 931–952 (2003).
- Acke, B. & van den Ancker, M. E. Resolving the disk rotation of HD 97048 and HD 100546 in the [O I] 6300  $\text{\AA}$  line: evidence for a giant planet orbiting HD 100546. *Astron. Astrophys.* **449**, 267–279 (2006).
- van der Plas, G. *et al.* The structure of protoplanetary disks surrounding three young intermediate mass stars. I. Resolving the disk rotation in the [O I] 6300  $\text{\AA}$  line. *Astron. Astrophys.* **485**, 487–495 (2008).
- Salyk, C., Blake, G. A., Boogert, A. C. A. & Brown, J. M. High-resolution 5  $\mu\text{m}$  spectroscopy of transitional disks. *Astrophys. J.* **699**, 330–347 (2009).
- Pontoppidan, K. M. *et al.* Spectroastrometric imaging of molecular gas within protoplanetary disk gaps. *Astrophys. J.* **684**, 1323–1329 (2008).
- van der Plas, G. *et al.* Evidence for CO depletion in the inner regions of gas-rich protoplanetary disks. *Astron. Astrophys.* **500**, 1137–1141 (2009).
- Pontoppidan, K. M., Blake, G. A. & Smette, A. The structure and dynamics of molecular gas in planet-forming zones: a CRIRES spectro-astrometric survey. *Astrophys. J.* **733**, 84–100 (2011).
- Sacco, G. G. *et al.* High-resolution Spectroscopy of Ne II emission from young stellar objects. *Astrophys. J.* **747**, 142 (2012).
- Piétu, V., Gueth, F., Hily-Blant, P., Schuster, K.-F. & Pety, J. High resolution imaging of the GG Tauri system at 267 GHz. *Astron. Astrophys.* **528**, A81–A95 (2011).

29. Beck, T. L. *et al.* Circumbinary gas accretion onto a central binary: infrared molecular hydrogen emission from GG Tau A. *Astrophys. J.* **754**, 72–77 (2012).
30. Regály, Z., Juhász, A., Sándor, Z. & Dullemond, C. P. Possible planet-forming regions on submillimetre images. *Mon. Not. R. Astron. Soc.* **419**, 1701–1712 (2012).

**Supplementary Information** is available in the online version of the paper.

**Acknowledgements** This paper makes use of the following ALMA data: ADS/JAO.ALMA#2011.0.00465.S. ALMA is a partnership of the ESO, NSF, NINS, NRC, NSC and ASIAA. The Joint ALMA Observatory is operated by the ESO, AUI/NRAO and NAOJ. This work was also based on observations obtained at the Gemini Observatory. Financial support was provided by Millennium Nucleus P10-022-F (Chilean Ministry of

Economy) and additionally by grant FONDECYT 1100221 and grant 284405 from the European Union FP7 programme.

**Author Contributions** General design of ALMA project, data analysis and write-up: S.C. Discussion of infrared observations of gas in cavities: G.v.d.P. Hydrodynamical modelling: S.P.M. ALMA data reduction: A.H. and E.F. Infrared-image processing: D.M., J.H. and J.H.G. Contributions to ALMA Cycle 0 proposal: A.J., F.M., D.W. and A.M.H. Design of ALMA observations: A.W., A.H. and S.C. Authors W.R.F.D. to A.W. contributed equally. All authors discussed the results and commented on the manuscript.

**Author Information** Reprints and permissions information is available at [www.nature.com/reprints](http://www.nature.com/reprints). The authors declare no competing financial interests. Readers are welcome to comment on the online version of the paper. Correspondence and requests for materials should be addressed to S.C. ([scasassus@u.uchile.cl](mailto:scasassus@u.uchile.cl)).